Available online at www.sciencedirect.com
ScienceDirect
Journal of Photochemistry and Photobiology A: Chemistry 189 (2007) 314–321
Journal of Photochemistry and Photobiology A:Chemistry
www.elsevier.com/locate/jphotochem

Preparation of TiO_2 nanocrystalline with 3–5 nm and application for dye-sensitized solar cell

Jinting Jiu [a,*], Seiji Isoda [a], Motonari Adachi [b], Fumin Wang [c]

[a] *The Institute for Chemical Research, Kyoto University, Uji, Kyoto 611-0011, Japan*
[b] *The International Innovation Center, Kyoto University, Yoshida-Honmachi, Sakyo, Kyoto 606-8501, Japan*
[c] *School of Chemical Engineering and Technology, Tianjin University, Tianjin 300072, PR China*

Received 2 August 2006; received in revised form 12 January 2007; accepted 20 February 2007
Available online 23 February 2007

Abstract

Nanocrystalline TiO_2 with 3–5 nm in diameter was prepared with a surfactant-assisted sol–gel method. The microstructure measured by XRD and high resolution TEM was pure high crystallinity anatase phase. Dye-sensitized solar cells were assembled using the prepared nano-scale TiO_2 crystals and its photocurrent–voltage performance was investigated. The electrodes give significantly higher Jsc when compared to the cell that fabricated by big particles. Also the effect of the particle size, surface area, pore structure and the film formation temperature on the performance of cells is discussed.

Keywords: Dye-sensitized solar cell; TiO_2 nanocrystal; Character; Preparation; Pore structure; Dye adsorption; Sintering temperature

1. Introduction

Recently, considerable attention has been paid on the synthesis and application of nanocrystalline materials, because of their novel and spectacular physical and chemical properties. These particular properties are resulted from the ultrafine structures (i.e., grain sizes smaller than 50 nm) of these materials and can be classified in two categories: properties that are relative to the bulk and to the surface. By employing this very high surface area, Grätzel group has successfully developed a new type of solar cell that is based on a nanocrystal mesoporous TiO_2 film electrode coated with a monolayer of sensitizer-dyes for light absorption and electron injection into the TiO_2 conduction band. The dye-sensitized solar cells (DSSC) are immediately derived and regarded as a regenerative low-cost alternative cells to conventional semiconductor devices, and then they have attracted considerable academic and practical interests [1–4]. In the cells [1,2], undoubtedly mesoporous titania film and dye are two of the key components for high power-conversion efficiency. Research efforts have focused on improving this system by creating a suitable porous structure or porosity in the mesoporous TiO_2 film with variety in particle size and morphology of TiO_2 [5], optimizing the fabrication and structure of TiO_2 film [6–9], developing new sensitizers [10], suppressing charge recombination [11] and improving interfacial energetics [12]. However, in the photoelectrochemical cell applications, TiO_2 film with large surface area, coated by light sensitizing dye molecules, is needed to be high crystallinity without crack and cavities and favorable electrical contiguity to a conducting glass substrate, so that dyes can be sufficiently adsorbed and electrons can be quickly transferred. Accordingly, TiO_2 film plays an essential role with respect to the efficiency.

Generally, TiO_2 electrode is made from nanocrystalline titania which is prepared by a sol–gel process or commercially available titania such as P-25. The former, sol–gel process, is highly potential as appropriate process for preparing nanostructure materials because the particle size, morphology and porosity can be controlled by adjusting preparation parameters. For example, Li et al. [13] prepared pure anatase type TiO_2 nanoparticles with the diameter of 100 nm by using titanium butoxide in butanol by a sol–gel method. However, the film electrode showed nearly the same efficiency comparing a film

* Corresponding author. Tel.: +81 774 38 3052; fax: +81 774 38 3055.
E-mail addresses: jiu@eels.kuicr.kyoto-u.ac.jp (J. Jiu), isoda@eels.kuicr.kyoto-u.ac.jp (S. Isoda), adachi@iae.kyoto-u.ac.jp (M. Adachi).

1010-6030/$ – see front matter © 2007 Elsevier B.V. All rights reserved.
doi:10.1016/j.jphotochem.2007.02.021

electrode consisted of P-25 with a typical size of 25 nm. They pointed out that the particle with large size decreased the internal surface and consequently worsened the cell performance but there are two advantages of the sol–gel layers which compensate the negative effect. One is the easiness in electrolyte diffusion within the layer, which is enhanced due to a gradient in the porosity of TiO_2 film. The other is the well-defined crystal structure of the sol–gel layers; pure anatase. Also they suggested that the preparation techniques of the nanocrystalline TiO_2 film is still a wide variety to realize high efficiency in DSSC. Later, Kambe et al. [14] synthesized single-phase anatase TiO_2 nanocrystals by a direct hydrolysis of titanium butoxide in organic solvent under high pressure and high temperature (150–300 °C). The photovoltaic property of the highly transparent cell composed of 13 or 11 nm particles with 16 μm film thickness was superior to that of P-25 film with 11 μm film thickness. Grätzel and coworkers [1,2,5] used TiO_2 nanoparticles of 10–15 nm, which were prepared by a hydrothermal method, as an electrode for DSSC. This electrode was sensitized by black dye, showing a high conversion efficiency (η) of 10.4% [15]. In contrast to that, another method for the formation of TiO_2 film electrode is the direct use of commercially available P-25 titania. Although Ito et al. [16] have investigated extensively the formation process and coating technique of P-25 film, the conversion efficiency could not over 7%. Except the composition of P-25 including 30% rutile structure, other factors, such as the crystallinity, porosity and crystal size are also key points to be optimized. In particular, the size of particles is known to be important, which determines the pore size, porosity and surface area of particle and is the crucial point for the adsorption of sensitizing dye molecules in DSSC. And it seems that smaller particles could be expected to achieve higher conversion efficiency in the DSSC. However, so far, TiO_2 electrodes composed of below 10 nm nanoparticles have been scarcely reported in the DSSC [9]. We have successfully prepared a nanocrystalline TiO_2 electrode with a diameter of 3–5 nm by a mixed template method, in which we found that the mixed template method can control the particle diameter and improve the film structure [9]. In this letter, we report DSSC performance of nanocrystalline TiO_2 electrodes as function of sintering temperature and film thickness in comparision to the P-25 electrodes. This study is essentially important to optimize the calcination process of nanocrystal particles and mesoporous film, and to make clear the relationship among the particles size, the surface area and the dye adsorption. We also discuss how the particle-size distribution influences the pore-size distribution in the film, which, in turn, affects the electrolyte transport phenomena and consequently the total efficiency in the cell.

2. Experimental

2.1. Colloidal synthesis

Typical synthesis of the nanocrystal TiO_2 has been described in our previous work [9] in the mixed template system of surfactant cetyltrimethylammonium bromide (CTAB) and copolymer F127 (poly(ethylene oxide)$_{106}$–poly(propylene oxide)$_{70}$–poly(ethylene oxide)$_{106}$). In that case, we found that the gel state is always affected by the addition of the surfactants that can control the diameter of particles in the system. However, the nanocrystalline TiO_2 can be also obtained simply with only F127, even though the particle size cannot be minimized as the mixed template. In order to examine DSSC performance as a function of sintering conditions, we selected copolymer F127 as single template to prepare the nanocrystals by fixing the pH value with HCl solution. The detail process is as the following. Six grams of template F127 was firstly added into 60 mL distilled water by mixed with 0.2 g of 2 M HCl for complete dissolution. And then an orange-color mixture solution of 6.8 g of tetraisopropylorthotitanate (TIPT) and 2.4 g of acetylacetone (ACA) was poured into the above F127 acid solution. The immediately formed yellow precipitation was stirred at 40 °C until a uniform transparent yellow solution was obtained. And the color of the above solution is generally lightened with the reaction time due to the hydrolysis of isopropyl groups in TIPT under the acid condition. Then the resulting bright yellow solution was kept at 80 °C in a closed container for over 3 days and a bright yellow, transparent, soft and stable TiO_2 gel was formed. Neither separation nor supernatant could be observed even after the gel was leaved in the 80 °C oven over 2 months.

2.2. TiO_2 electrode preparation

For preparation of photoelectrodes, normal doctor blade technique was applied to fabricate the TiO_2 film [9]. Firstly, the gel was stirred to form an easily mobilized gel and then a little of the gel was spread onto a conducting glass substrate (ITO, Geomatec Co. LTD, sheet resistance is 5 Ω/□) in advance surrounded with a adhesive tapes (Scotch, ∼40 μm thickness) as spacers. The layer was dried at 40 °C for several minuets, followed by treatment at a determined sintering temperature for 10 min in an oven. And then the hot film was taken out from the oven and kept at room temperature for several minuets. Successively further layers were coated on the hot film and dried and calcined for 10 min each. A designed thickness of TiO_2 films can be fabricated by the repetitive coating–calcining process. At last, the film was calcined for various fixed times to compare the performance of cell. Covering of the TiO_2 surface with dye was carried out by soaking the film for over 12 h in a solution of N719 dye (Solaronix). The dye-adsorbed TiO_2 electrode was assembled into a sandwich-type cell with a counter electrode (platinum-sputtered ITO glass) by clamps. A drop of electrolyte solution (0.1 M LiI, 0.6 M DMPII (1,2-dimethyl-3-*n*-propylimidazolium iodide), 0.05 M I_2, and 0.5 M TBP (4-*tert*-butylpyridine) in methoxyacetonitoryl) was introduced into the clamped electrodes.

In order to observe the microstructure of the obtained nanocrystal TiO_2, the films before and after adsorption of the dye were peeled off from the glass substrate and dispersed into ethanol, and then a drop of the solution was put on a grid covered with carbon film for the observation by transmission electron microscopy (TEM). The X-ray diffraction (XRD) pattern was obtained by measuring directly the calcinated film on the glass substrate. The sample for nitrogen adsorption–desorption was prepared by drying the gel on an open container with 1–2 mm

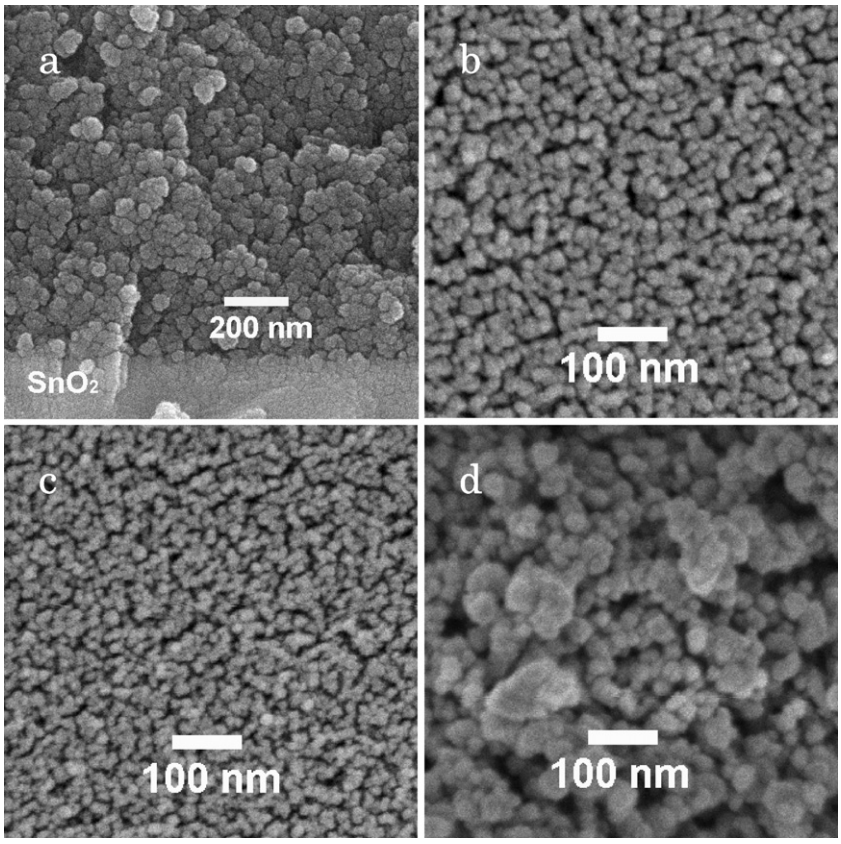

Fig. 1. SEM images of the cross-section (a), the surface morphology of TiO_2 film calcined at 550 °C (b) and 350 °C (c), the surface morphology of P-25 film (d).

thickness at 80 °C oven for 1 week and calcining at fixed temperatures for 2 h.

The average crystallite size was calculated according to the Scherrer equation from XRD. Brunauer–Emmett–Teller (BET) surface area (S_{BET}) was determined using a BEL SORP 18 PLUS nitrogen adsorption apparatus after all samples were degassed at 100 °C for 4 h. The morphology and thickness of the mesoporous TiO_2 electrodes were characterized by scanning electron microscopy (SEM; JEOL, JSM-5510). Photocurrent–voltage measurements were performed using an AM 1.5 solar simulator (100 mW/cm^2, Bunkoh-keiki CEP-2000Model, Japan). The cell size was 0.25 cm^2. The cells made of P-25, a commercial TiO_2 containing anatase and rutile phase, were also prepared for comparison.

3. Results and discussion

3.1. Characterization of nanocrystalline TiO_2 film

Fig. 1 shows the SEM images of the cross-section and the surface morphology of TiO_2 film. Fig. 1a indicates that any crack and gap is not observed in the film although it has been formed by several-times coating. Also the surfaces are very smooth and homogeneous without cavities and cracks (Fig. 1b and c) comparing the surface of P-25 cell (Fig. 1d). The P-25 cell appears to have big agglomerates constructed by many nanoparticles except individual particles, resulting in high roughness. Hence, it is very difficult to obtain clear SEM images with large magnification (Fig. 1d). And the packing structure of large and small particles will affect the pore diameter and volume of the film as discussed in the following. Fig. 1b and c show the surface morphology of TiO_2 film calcined at 550 and 350 °C, respectively, and the calcined temperature does not affect the surface morphology of TiO_2 film except the slight increasing in particle size. Since no clear changes are observed in the film roughness, porous structure, the copolymer F127 template effectively avoids crack in the film, maintains the homogeneity and also prevents the large aggregation of particles in coating and calcination. Especially, the burning and decomposition of the templates in calcinations make the film directly a porous structure which is simple and suitable for the formation of solar cell electrode. It is worth to be noted that the surface images show a clear network structure composed of small particles connected with each other, which can be attributed to the use of copolymer F127 for the preparation of mesoporous materials [17]. And the network structure has indicated enhanced performance in DSSC due to the huge surface area [18] and optimum pore diameter and pore volume [19].

XRD patterns of the TiO_2 film calcined at different temperatures are shown in Fig. 2 together with that of P-25 films. Peak 2 and 3 are diffraction peaks from the substrate. Diffraction signal assigned to the anatase (1 0 1) structure at 25.3° (peak 1) is clearly observed in both TiO_2 and P-25 films. The diffraction signal at 27.5° due to the rutile phase (1 1 0) is not observed in TiO_2 films except for P-25 film. The intensity ratio of the diffraction peaks figure out ca. 20% content of rutile in the P-

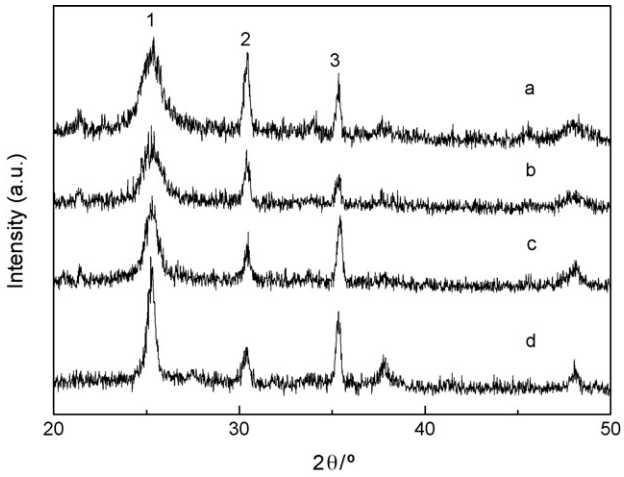

Fig. 2. XRD patterns of TiO_2 films calcined at 350 °C (a), 450 °C (b), 550 °C (c) and P-25 film (d).

Table 1
Physicochemical property of TiO_2 films with different calcining temperatures

Temperature (°C)	Crystallite size (nm)	S_{BET} ($m^2\ g^{-1}$)	Pore volume ($ml\ g^{-1}$)	Pore size (nm)
350	3.9	151.8	0.404	3.17
450	5.3	106.2	0.400	5.49
550	7.9	77.8	0.346	5.49
P-25	23	58	0.291	1.04

25 film. Absence of the diffraction due to rutile phase in the TiO_2 films means that the sintering process in the film fabrication does not affect the crystalline phase itself even at a high temperature of 550 °C. As for the width of peaks and intensity of diffraction signals with different calcining temperatures, the diffraction intensity slightly increases and the width decreases with the calcining temperature, which suggests the increases in crystallinity and particles size. However, the half-height widths of the diffraction peaks of TiO_2 films, which are responded to the sizes of particles, are very wider than that of P-25 even at high calcination temperatures. Table 1 shows the size of particles calculated by Scherre's equation. The particles sizes are 3.9, 5.3 and 7.9 nm calcined at 350, 450 and 550 °C, respectively. The XRD pattern showed a big change in size and crystallinity of TiO_2 particles when the temperature was over 550 °C (not shown here). Fig. 3 shows the morphology of TiO_2 particles that were peeled from glass substrates with different calcined temperatures. They reveal that the nanoycrystals have an irregular spherical shape with a size distribution of 3–5 nm. With increasing temperature, the irregularity (deviation from spherical shape) is enhanced and even evolved into a clear hexagon shape particle with high crystallinity. Furthermore, the diameter of particles is increased to 3–8 and 3–10 nm at 450 and 550 °C, respectively, even though large particles were observed occasionally at such temperatures. This fact agrees well with that expected from XRD data and observed from SEM images. At 350 °C, the randomly packed particles show many grain boundary among the particles, which indicates the low crystallinity in these parts. With increasing temperature, the boundary becomes clear and sharp as shown by lattice fringes in the TEM images (Fig. 3c, white arrows), suggesting that the crystallinity of particles is improved and enhanced with the heat energy. From XRD and TEM observations, the TiO_2 nanoparticles are primary particles with excellent dispersivity and stability at 350 °C. With increasing temperature, the diameter of particles is slightly increased with improved interconnection between the particles. However, the diameter of major main particles is still lower than 10 nm in all cases. We deduce that the copolymer template plays a key role for keeping the size of TiO_2 particles after and before calcination. In the present case, copolymer F127 promotes the homogeneity of the mixture solution and avoids the large aggregation and recombination of TiO_2 crystalline nucleuses in the formation and calcination processes, just as reported in literature [20].

On the other hand, it should be noted that the necking regions (typically shown in Fig. 3b, white ellipses) between the particles are benefit for the formation of network structure as observed in SEM images, which is expected to be advantageous for the transport of electrons in the skeleton comparing films packed simply with single particles. The necking regions are developed with the heat energy by the heat-melting growth or coalescence between particles, which is also evidenced by the formation of large particles observed in TEM images with increasing temperature.

3.2. Performance of solar cells based on the nanocrystalline TiO_2 film

Fig. 4 shows that the amount of the dye adsorbed on the TiO_2 nanocrystalline film formed at 450 °C is more than twice as much as on the P-25 film at the same thickness. And the dye amount

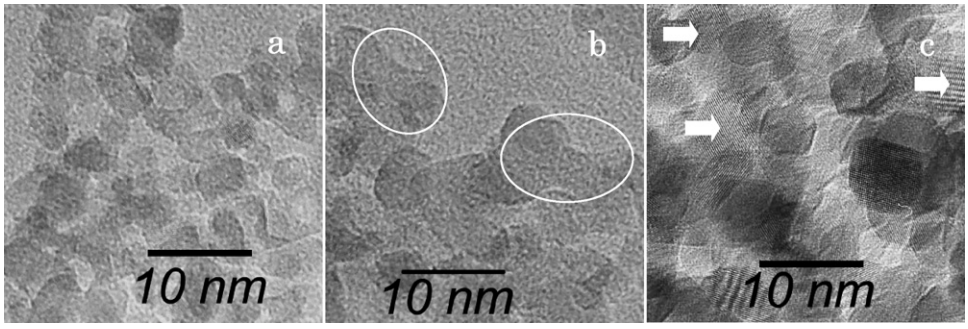

Fig. 3. TEM images of TiO_2 particles peeled from calcined films at 350 °C (a), 450 °C (b), and 550 °C (c).

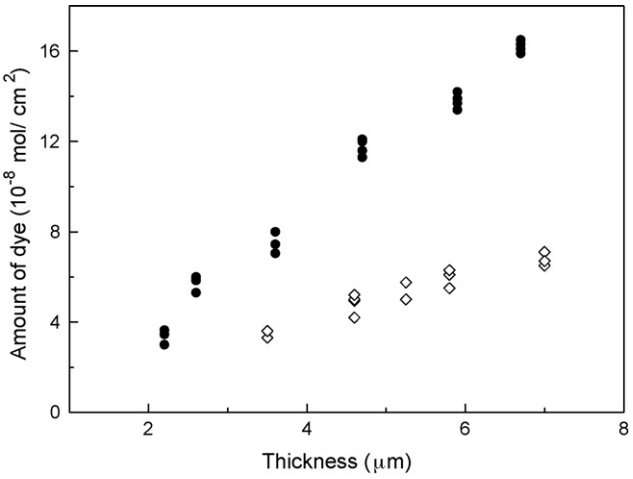

Fig. 4. Dependence of amount of dye on the thickness of film of nanocrystalline TiO_2 (●) and P-25 (◊).

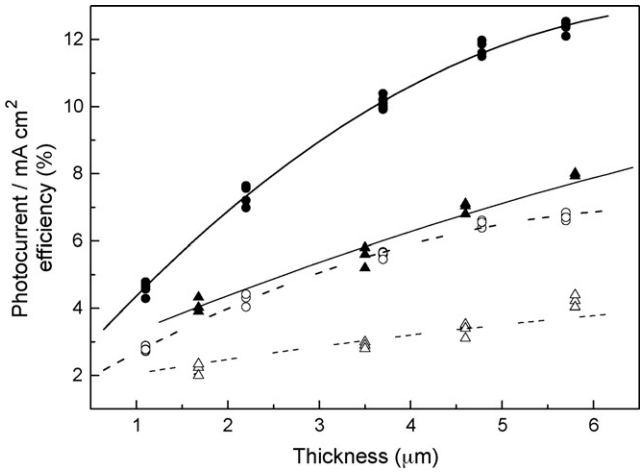

Fig. 5. Dependence of photocurrent density (closed marks) and efficiency (open marks) on the thickness of films: nanocrystalline TiO_2 (cycle) and P-25 (triangle).

is nearly proportional to the thickness of the both TiO_2 films but the slope is smaller for the P-25 films. Also the dye amount adsorbed in the nanocrystalline TiO_2 film is clearly higher than those TiO_2 films reported in Grätzel group [1], which is about 1.3×10^{-7} mol cm^{-2} with the film thickness of 10 μm.

The effect of sintering temperature on the dye adsorption was also examined. The amounts of dye on a film with the thickness of 4.3 μm are 1.25, 1.07 and 0.89×10^{-7} mol cm^{-2}, when sintered at 350, 450 and 550 °C, respectively. Slight decrease in the dye adsorption with increasing sintering temperature may reflect the decrease in the surface area of films owing to the necking parts between particles and also larger particles size, which is agree with the analysis of nitrogen isotherm shown in Table 1 and SEM, and TEM observation. When the sintering temperature is increased, the surface area is drastically decreased from 151 to 77.8 m^2 g^{-1} as shown in Table 1. From the SEM and TEM images, it can be found that the diameter of particles is slightly increased by increasing sintering temperature but the interconnection between particles is highly improved. The interconnection is the major reason of decreased in the dye amount adsorbed on the nanocrystalline TiO_2 film at higher temperatures. The amount of dye on nanocrystalline TiO_2 film is nevertheless very higher than that on P-25 films even at high sintering temperature, which is attribute to the bigger surface area and higher crystallinity of nanocrystalline TiO_2 film.

The performance of the DSSC can be characterized by measuring the current–voltage curves of the prepared DSSC from which the light-to-electricity conversion efficiency can be calculated. Fig. 5 shows the dependence of the conversion efficiencies (η) and photocurrent density on the thickness of nanocrystalline TiO_2 films prepared at 450 °C. Each measurement was carried out using three to six samples to confirm the reproducibility. The photocurrent density of the TiO_2 films dependes on the thickness of the films. As the thickness of the TiO_2 film increases from 1.1 to 5.7 μm, photocurrent density increases from 4.6 to 12.5 mA cm^{-2}. For the P-25 film the photocurrent density is lower and increases from 4.1 to 7.9 mA cm^{-2} when the thickness of film increased from 1.7 to 5.9 μm. And it can be found that the increase in the photocurrent density becomes slower when the thickness is over 5 μm in the two cases. On a parallel with the above, the conversion efficiency of the two cases shows similiar increasing trend with the thickness of films. A 6.8% efficiency is achieved based on the nanocrystalline TiO_2 film with the thickness of 5.7 μm. However, the highest efficiency obtained in P-25 films is lower with only 4.2% although the thickness is almost the same.

It should be noted here that the thin nanocrystalline TiO_2 film (2.2 μm) shows the same photocurrent density (7.9 mA cm^{-2}) as the thick P-25 film (5.9 μm), while the former chemisorbes about one-half of the latter in the dye molecules (Fig. 4). To evaluate the efficiency of the dye molecules which generate photocurrent, the photocurrent values are plotted as a function of the amount of dye per unit area of the films in Fig. 6. Photocurrent density increased almost linearly with the amount of dye molecules, but saturation of the photocurrent density is observed at large values of the dye adsorbed in the films (over 1×10^{-7} mol cm^{-2}). The saturation tendency in P-25 film happens faster at the amount

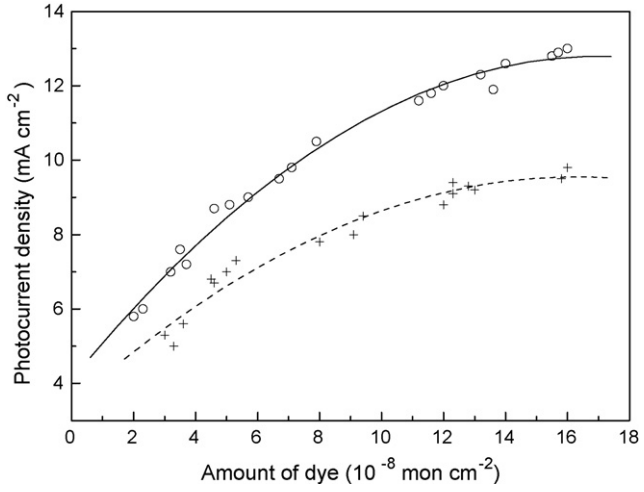

Fig. 6. Dependence of photocurrent density on the amount of dye on nanocrystalline TiO_2 films (◯) and P-25 films (+).

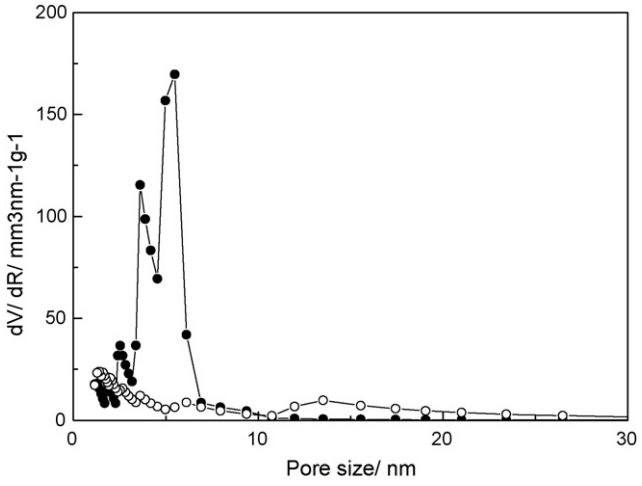

Fig. 7. Pore-size distribution of nanocrystalline TiO_2 films (●) and P-25 films (○).

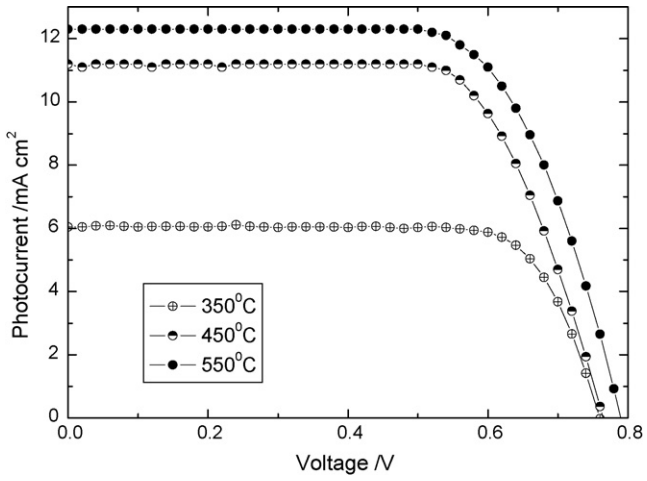

Fig. 8. Photocurrent–voltage curves of nanocrystalline TiO_2 films calcined at different temperatures.

of dye with 0.8×10^{-7} mol cm^{-2}. And the higher photocurrent density is always observed for nanocrystalline TiO_2 films not for P-25 film.

On the other hand, the nanocrystal TiO_2 film and P-25 film show a remarkable difference in their pore-size distribution shown in Fig. 7 at the sintering temperature of 450 °C. P-25 film has the main distribution at very small pores below 5 nm, the maximum of the curves is found at 1.4 nm in addition to the large pores distributed weakly in the range of 11–18 nm (Fig. 7). Differently, the nanocrystal TiO_2 film has a slight larger pore-size distribution in the range of 3–7 nm in which the diameter of 5.57 nm corresponds to the maximum distribution. The character of small pore-size distributions explains the low efficiency in the P-25 film, because the diffusion of I_3^- ion in electrolyte becomes a slow and limits the current production [21]. The second reason is due to the lower pore volume compared to nanocrystal TiO_2 film. Although P-25 film includes also large pores even larger than 20 nm, the pore volume is too small to dominate the main steps.

The effect of sintering temperature on the performance of cell was also examined. Fig. 8 shows the photocurrent–voltage curves of nanocrsystal TiO_2 films calcined at 350, 450 and 550 °C. Clearly the high temperature realizes high photocurrent and high conversion efficiency of light-to-electricity. However, the thickness of film is largely different although these films were fabricated with the same five-times coating by doctor blade method mentioned already. Usually, every coating can generate one pre-film with a thickness of about 30–40 μm before calcination. The thickness of film is 6.7, 5.5 and 4.3 μm when fabricated at 350, 450 and 550 °C, respectively. Therefore, it can be concluded that the resulted-thickness of film for every coating is about 0.86, 1.1 and 1.34 μm with decreasing sintering temperature, which suggests that the thick film could be obtained at low sintering temperature. However, thin film calcinated at high temperature achieves high efficiency in the DSSC. We have mentioned that such a film can adsorbed smaller amount of dye than that formed at low temperature, indicating that the film structure, not the thickness may play a key role in DSSC. Zukalova et al. [18] have also reported that the performance of DSSC fabricated with organized mesoporous TiO_2 film is expected to be improved, if the crystallinity of the mesoporous TiO_2 skeleton is enhanced by high sintering temperature. In our case, the increasing temperature leads to the formation of high crystallinity coalescenced film shown in TEM, SEM and XRD measurements, which improves the network structure of film and enhances the interconnection between particles resulting in the swift diffusion of electrolyte and good transport of electrons in the film. Furthermore, the high temperature also decreases the amount of impurity, for example, carbon residues remained when copolymer F127 is burned. Such impurity generally makes worse the crystallinity of oxide and generates the trapping opportunities for the electrons. At last, we have to mention the effect of pore-size distribution with different sintering temperatures shown in Fig. 9. In Fig. 9, the main difference in the pore-size distribution is observed in the range around 4.2 nm at 350 °C. With increasing sintering temperature, the pores are enlarged from 3 to 6.3 nm before adsorption of dye molecules. When a pore with 3 nm diameter is occupied by the dye layer (dye

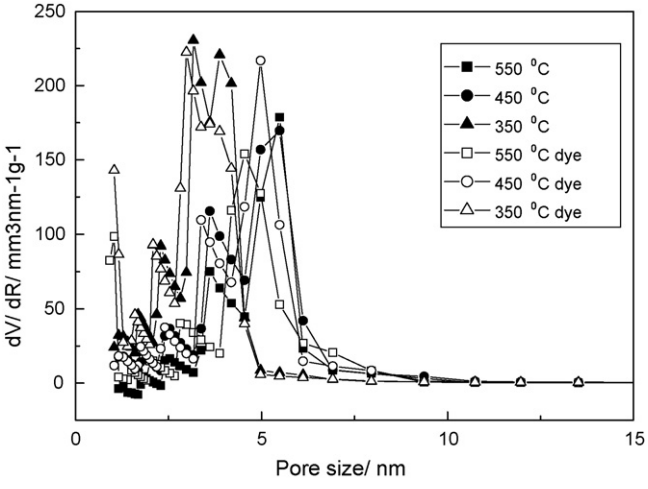

Fig. 9. Pore-size distribution of nanocrystalline TiO_2 films before (closed marks) and after (open marks) adsorption of dye molecules.

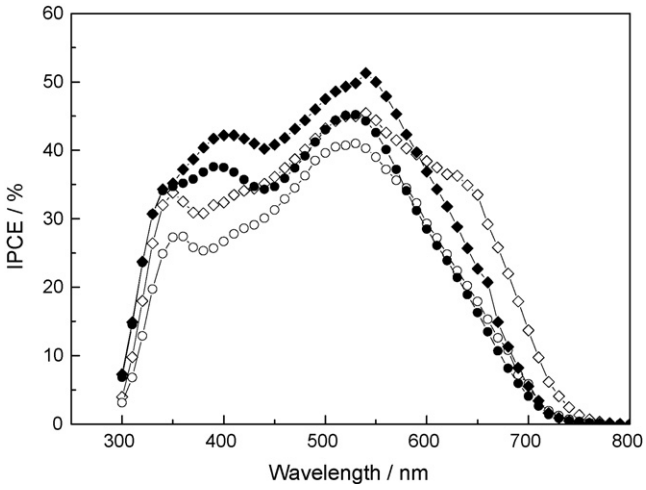

Fig. 10. The IPCE spectra of TiO_2 films (●: 2.2 μm; ♦: 3.9 μm) and P-25 films (◯: 5 μm; ◇: 10.8 μm).

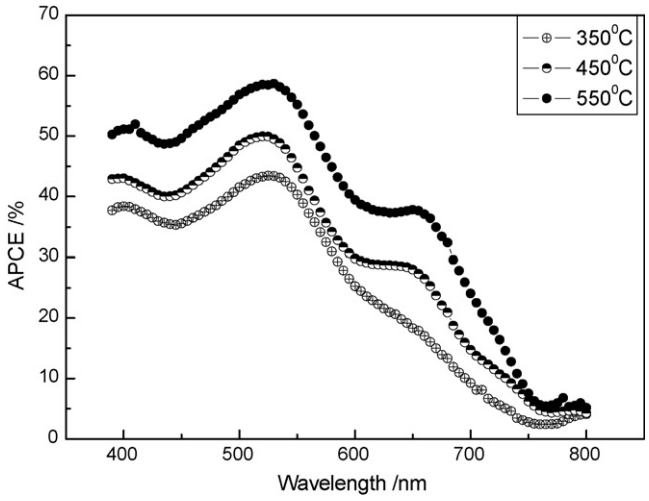

Fig. 11. The APCE spectra of nanocrystalline TiO_2 films calcined at different temperatures.

molecular diameter is 1.5 nm) that is adsorbed on the pore wall, an empty space of only 1 nm for the diffusion of the electrolyte. This happens in the film calcined at 350 °C films, because the pore size at the maximum distribution is about 4 nm. This space is very similar to the size of the I_3^- ion, so that the diffusion kinetics in the electrolyte becomes a limiting step resulting in a drastic influence on the efficiency [21]. Contrastly, the size of pore after dye molecules is enough for the transport of I_3^- ion even considering their solvation shell in the cases of 450 and 550 °C films. It is clear the efficiency is increase with increasing pore size; i.e., nanocrsystal TiO_2 films calcined at 550 °C with large pore size (5.49 nm) has higher efficiency than other films with small pore size (Figs. 8 and 9). The same results have been also reported by Karthikeyan et al. [19]. They suggested that only surface area of the film alone is not sufficient, the pore volume and pore diameter are also important in determining the overall performance of the DSSC. However, the pore distribution indicates no clear difference at 450 and 550 °C films, and then other parameters, such as the crystallinity would affect the efficiency at high sintering temperatures.

And it should be mentioned that the TiO_2 films composed of very small particles are fully transparent irrespective to the thickness and sintering temperature, while P-25 film is translucent or opaque depending on the thickness. Hence the scattering of light due to large particles does not play a role in the photovoltaic response of the nanocrystalline TiO_2 film systems comparing the systems consisted of P-25 film. The IPCE spectra (Fig. 10) indicates the effect due to scattering of light. Since the IPCE values are drastically increased in the long wavelength region (650–750 nm) in P-25 films (10.8 μm thickness), the enhanced IPCE is generally attributed to the light scattering effect in the region due to big particles. On the other hand, in such long wavelength region, the nanocrystalline TiO_2 film shows only lower IPCE value. However, in the short wavelength region (400–600 nm), high IPCE values are always achieved in the nanocrystalline TiO_2 film in particular for lower film thickness (2.2 and 3.9 μm in Fig. 10). The difference could be generally explained by the amount of adsorbed dye molecules. However, high IPCE value is also achieved with lower dye amount in the film with 2.2 μm thickness shown in Figs. 4 and 10. The results suggested that the dye amount is not a determined factor, and film structure mentioned above should be reconsidered in DSSC as pointed by Karthikeyan et al. [19]. Because the IPCE does not take into account the light harvesting efficiency of the solar cell, it is not well suited for detailed discussion of the photonto–current conversion processes; IPCE has to be converted to the absorbed photon-to-current conversion efficiency (APCE). APCE can be calculated by using of the spectra of IPCE and dye adsorption of film cells according to the method mentioned by Hara et al. [22], and the results is shown in Fig. 11. This clearly shows that the APCE value of nanocrystalline TiO_2 film calcined at high temperature is higher than that with lower sintering temperature. It is about 58, 50 and 43% at 525 nm for 350, 450 and 550 °C, respectively. It further indicates high temperature improved the film structure of nanocrystalline TiO_2 film resulting in high absorbed photon-to-current conversion efficiency (Table 2).

In addition to the pore structure affecting on the efficiency of nanocrystalline TiO_2 film, another parameter is the crystal structure. Generally, lattice imperfections in crystal such as impurities, vacancies or lattice dislocations, interfere with electron transport in semiconducting materials. Considering that P-25 is a mixture of ca. 80% anatase and ca. 20% rutile nancrystallites (Fig. 2), the high photocurrent generation in the nanocrystalline TiO_2 film suggests that the transport of photoinjected electrons should become effective in the single phase anatase TiO_2 film agglomeration.

Table 2
Photovoltaic properties of TiO_2 cells

Temperature (°C)	Thickness of film (μm)	Jsc (mA cm^{-2})	Voc (V)	Fill factor	Efficiency (%)
350	6.7	6.03	0.76	0.764	3.5
450	5.5	11.1	0.766	0.706	6
550	4.3	12.3	0.79	0.710	6.9

On the other hand, grain boundaries between the particles should affect the electron transport of injected electrons as well as the crystallinity of the particles themselves. The atomic arrangement of nano-scale materials is unlike to that seen in bulk crystals because of the large volume fraction (greater than 50%) in grain boundaries or interfaces. Coarse-grained materials have less than 3% of all atoms associated with grain boundaries or interfaces, while the materials with nano-sized grains allocate 5–50% of all atoms. Grain boundaries in polycrystals are known to play significant roles on the materials properties. For example, varistor ceramics prepared from nano-size particles always produce a more homogenous, smaller and regular grain size, and a cleaner and closer grain boundary microstructure. These characteristics are related to a higher breakdown voltage, smaller leakage current, larger nonlinear coefficient, smaller dielectric constant and dielectric loss than conventionally produced varistors [23]. The present system of the nanocrystalline TiO_2 electrodes is consisted of several nm crystallites, and thus contains a significant amount of grain boundaries with homogenous microstructure and small grain size as shown in TEM images. The high efficiency of the nanocrystalline TiO_2 electrodes implies that not only the single and pure phase anatase crystalline structure but also the smooth neck connection at the grain boundaries should contribute to the effective electron transport in the DSSC [23]. Linear increment of photocurrent density depending on the thickness of the TiO_2 films (Fig. 6) also supports the formation of the effective crystalline neck connection in the thicker agglomeration. As for the template of copolymer F127, the gradual elimination might contribute to the formation of homogeneous grain boundaries with neck-like connection during sintering of the agglomeration. In such a way, improvement of the efficiency in the nanocrystalline TiO_2 films sintered at high temperature is observed (Fig. 8), which should be also contributed to the effective crystalline neck-connection at high temperature although it has small surface area.

With the nanocrystalline TiO_2 film, 7.54% conversion efficiency, with the open circuit photovoltage of 759 mV, the short circuit photocurrent of 13.5 mA/cm^2, and the fill factor 0.748, has been obtained with the nanocrystalline TiO_2 film of 6 μm in thickness fabricated at 550 °C. However, higher efficiency is difficult to be achieved with only the nanocrystalline TiO_2 film composed of these very small nanoparticles and the sensitizer dye of N719 due to the low light harvest in the red region. As it has been suggested that the TiO_2 photoelectrode morphology, made of layers of nanoparticles, light-scattering particles, and mixture of nanoparticles and light-scattering particles on the conductive glass at a desirable sequence and thickness, is essential and necessary for high efficiency [24], an optimum film morphology composed of the small nanoparticles and scattering particles has been studied in the our recent work. However, the small nanocrystals adsorbed much more sensitizer will be a notable item for improvement of DSSC performance.

4. Conclusions

Nanocrystalline TiO_2 with 3–5 nm in diameter, high surface area and single-phase anatase structure, has been synthesized with a surfactant-assisted sol–gel method. Porous TiO_2 film with narrow pore-size distribution and high transmittance were successfully formed and applied in DSSC. The electrochemical characters and dye-adsorption depended on the surface area and structure of film, which is influenced by the fabrication conditions such as sintering temperature, coating times, thickness, and crystallinity of particles.

Acknowledgements

This work was supported by the Strategic University/Industry Alliance of the International Innovation Center, Kyoto University. The conductive ITO was kindly donated by Geomatec Co. Ltd.

References

[1] M.K. Nazeeruddin, A. Kay, I. Rodicio, R. Humpbry-Baker, E. Miiller, P. Liska, N. Vlachopoulos, M. Grätzel, J. Am. Chem. Soc. 115 (1993) 6382.
[2] U. Bach, D. Lupo, P. Comte, J.E. Moser, F. Weissörtel, J. Salbeck, H. Spreitzer, M. Grätzel, Nature 395 (1998) 583.
[3] K. Tennakone, G.R.R.A. Kumara, I.R.M. Kottegoda, V.P.S. Perera, J. Chem. Soc. Chem. Commun. (1999) 15.
[4] K. Hara, Y. Tachibana, Y. Ohga, A. Shinpo, A. Suga, K. Sayama, H. Sufihara, H. Arakawa, Sol. Energy Mater. Sol. Cells 77 (2003) 89.
[5] N. Papageogiou, C. Barb, M. Grätzel, J. Phys. Chem. B 102 (1998) 4156.
[6] M. Gómez, J. Lu, E. Olsson, A. Hagfeldt, C.G. Granqvist, Sol. Energy Mater. Sol. Cells 64 (2000) 385.
[7] R. Odríguez, J. Lu, E. Olsson, C.G. Granqvist, Adv. Mater. 12 (2000) 341.
[8] M. Adachi, Y. Murata, I. Okada, S. Yoshikawa, J. Electrochem. Soc. 150 (2003) G488.
[9] J. Jiu, F. Wang, M. Sakamoto, J. Takao, M. Adachi, J. Electrochem. Soc. 151 (2004) A1653.
[10] S. Ferrere, B.A. Gregg, J. Am. Chem. Soc. 120 (1998) 843.
[11] S.Y. Huang, G. Schlichthörl, A.J. Norzik, M. Grätzel, A.J. Frank, J. Phys. Chem. B 101 (1997) 2576.
[12] G. Schlichthörl, S.Y. Huang, J. Sprague, A.J. Frank, J. Phys. Chem. B 101 (1997) 8141.
[13] Y. Li, J. Hagen, W. Schaffrath, P. Otschik, D. Haarer, Sol. Energy Mater. Sol. Cells 56 (1999) 167.
[14] S. Kambe, K. Murakoshi, T. Kitamura, Y. Wada, S. Yanagida, H. Kominami, Y. Kera, Sol. Energy Mater. Sol. Cells 1 (2000) 427.
[15] M.K. Nazeeruddin, P. Péchy, T. Renouard, S.M. Zakeeruddin, R. Humphry-Baker, P. Comte, P. Liska, L. Cevey, E. Costa, V. Shklover, L. Spiccia, G.B. Deacon, C.A. Bignozzi, Grätzel, J. Am. Chem. Soc. 123 (2001) 1613.
[16] S. Ito, T. Kitamura, Y. Wada, S. Yanagida, Sol. Energy Mater. Sol. Cells 76 (2003) 3.
[17] D. Zhao, Q. Huo, J.L. Feng, B.F. Chmelka, G.D. Stucky, J. Am. Chem. Soc. 120 (1998) 6024.
[18] M. Zukalova, A. Zukal, L. Kavan, M.K. Nazeeruddin, P. Liska, M. Grätzel, Nanoletters 5 (2005) 1789.
[19] C.S. Karthikeyan, M. Thelakkat, M. Willert-Porada, Thin Solid Films 511–512 (2006) 187–194.
[20] S. Forster, M. Antonietti, Adv. Mater. 10 (1998) 195.
[21] C.J. Barbe, F. Arendes, P. Comte, M. Jirousek, F. Lenzmann, V. Shklover, M. Grätzel, J. Am. Ceram. Soc. 80 (1997) 3157.
[22] K. Hara, H. Horiuchi, R. Katoh, et al., J. Phys. Chem. B 106 (2002) 374.
[23] X. Kang, M. Tu, M. Zhang, T. Wang, Solid State Phenomena 99–100 (2004) 127.
[24] Z. Wang, H. Kawauchi, T. Kashima, H. Arakawa, Coord. Chem. Rev. 248 (2004) 1381.